# Multiscale approach to equilibrating model polymer melts

Carsten Svaneborg*
*University of Southern Denmark, Campusvej 55, DK-5230 Odense M, Denmark*

Hossein Ali Karimi-Varzaneh,† Nils Hojdis,‡ and Frank Fleck§
*Continental, PO Box 169, D-30001 Hannover, Germany*

Ralf Everaers‖
*Univ Lyon, ENS de Lyon, Université Claude Bernard, CNRS, Laboratoire de Physique and Centre Blaise Pascal, F-69342 Lyon, France*
(Received 7 June 2016; published 13 September 2016)

We present an effective and simple multiscale method for equilibrating Kremer Grest model polymer melts of varying stiffness. In our approach, we progressively equilibrate the melt structure above the tube scale, inside the tube and finally at the monomeric scale. We make use of models designed to be computationally effective at each scale. Density fluctuations in the melt structure above the tube scale are minimized through a Monte Carlo simulated annealing of a lattice polymer model. Subsequently the melt structure below the tube scale is equilibrated via the Rouse dynamics of a force-capped Kremer-Grest model that allows chains to partially interpenetrate. Finally the Kremer-Grest force field is introduced to freeze the topological state and enforce correct monomer packing. We generate 15 melts of 500 chains of 10.000 beads for varying chain stiffness as well as a number of melts with 1.000 chains of 15.000 monomers. To validate the equilibration process we study the time evolution of bulk, collective, and single-chain observables at the monomeric, mesoscopic, and macroscopic length scales. Extension of the present method to longer, branched, or polydisperse chains, and/or larger system sizes is straightforward.

DOI: 10.1103/PhysRevE.94.032502

## I. INTRODUCTION

Computer simulations of polymer melts and networks allow unprecedented insights into the relation between microscopic molecular structure and macroscopic material properties such as the viscoelastic response to deformation; see, e.g., [1–4]. Such simulation studies rely on very large model systems to reliably estimate material properties, and an important obstacle is the generation of large well equilibrated model systems for long entangled polymer chains.

What do we mean by equilibrium in the case of a linear homopolymer polymer melt? (1) Polymeric liquids have bulk moduli comparable to that of water, and they are nearly incompressible. Hence in equilibrium, we expect model melt states without significant density fluctuations. (2) Single chains in a melt adopt self-similar random walk statistics because excluded volume interactions are screened at length scales sufficiently large compared to monomeric scales. Hence in equilibrium, we expect model states without significant deviations from random walk statistics. (3) At mesoscopic scales, many polymer chains pervade the same volume, such that chains are strongly topologically entangled. This gives rise to the well known plateau modulus [5]. Hence in equilibrium, we also require model melts that achieve the correct entanglement density. (4) Finally at the monomeric scale we require the correct monomeric packing, such that we can expect to run long stable simulations where topology is preserved. Taken together, these constraints couple the conformations on scales that range from monomeric to macroscopic length scales. This makes the problem of making equilibrated model melts particularly difficult, and this problem is acerbated in the case of heteropolymers or for branched polymers which are of significant industrial interest.

Brute force equilibration of model polymer materials is typically not feasible. Polymer materials display dynamics over a huge range of time scales. Even for polymers of moderate size, their largest conformational relaxation times are many orders of magnitude beyond that which is currently available via brute force simulation. Monomeric motion takes place on picosecond time scales, whereas conformational relaxation times can easily reach up to macroscopic time scales. For a long linear polymer chain the dominant relaxation mechanism is reptation [6–8] which gives rise to relaxation times $\tau \sim N^3$ where $N$ is the number of monomers [7]. In the case of star shaped polymers, reptation is not possible and the dominant relaxation mechanism becomes contour length fluctuations [9], in which case the relaxation times are $\tau \sim \exp(N_{\mathrm{arm}})$, where $N_{\mathrm{arm}}$ is the number of monomers in an arm [10].

To our knowledge, there are three major strategies for equilibrating model polymer melts that address the challenges raised above: (a) algorithms that attempt to construct equilibrium model melts with the correct large-scale single chain statistics; (b) algorithms that utilize unphysical Monte Carlo (MC) moves to accelerate the dynamics compared to brute force molecular dynamics (MD), which simulates the real physical polymer dynamics; (c) algorithms using different models, e.g., utilizing softer potentials and a push-off process to allow chains to cross to accelerate the relaxation process.

*science@zqex.dk; http://www.zqex.dk/
†ali.karimi@conti.de
‡nils.hojdis@conti.de
§frank.fleck@conti.de
‖ralf.everaers@ens-lyon.fr

 

In the present approach we combine all these approaches, but before presenting our approach we review examples of these strategies found in the literature.

It is easy to generate single chain conformations with the desired large scale chain statistics. Equilibration procedures following this approach typically place the resulting chains randomly into the simulation domain. However, when monomer packing is introduced, the presence of density fluctuations in the initial state cause significant local chain stretching and compression. Brown *et al.* [11] were the first to recognize the importance of such density fluctuations. This was analyzed in detail by Auhl *et al.* [12], who made two proposals of how to resolve the density fluctuations, either to accelerate the relaxation utilizing double bridging moves, or to prepack the chains in space to avoid density fluctuations. This was done using Monte Carlo simulated annealing and accepting only moves that reduce density fluctuations [12].

A completely different approach is has been proposed by Gao [13]. The idea is to start by an equilibrated liquid of monomers and then to create bonds between the monomers corresponding to a melt of polymers. This completely sidesteps the issue of density fluctuations, since the monomeric liquid is also incompressible. However, the problem becomes how to identify a set of potential bonds to that correspond to a monodisperse melt of long linear or branched polymers. To reach near complete conversion Gao had to increase the search distance for the last bonds, and to remove the last monomers that could not be bonded. Whereas Gao performed instantaneous bonding on a frozen monomer liquid, Barrat and co-workers [14] extended the method by allowing the monomers to move during bonding. This has the effect of enhancing the search distance for bonding. This method still has issues with producing monodisperse melts, Barrat and co-workers solved the problem by aborting the bonding procedure when 80% of the monomers are linked into monodisperse chains, and then removing the last 20% of monomers. The resulting states were then compressed to the target pressure, which globally deforms the chain statistics.

Monte Carlo (MC) techniques have the advantage that unphysical moves can be used to accelerate the relaxation dynamics compared to MD techniques, which follow the physical dynamics. A key contribution to the equilibration of polymer melts has been the complex MC moves developed by Theodorou and co-workers [15,16]. End-bridging moves work by identifying an end monomer of one chain and an internal monomer of another chain where the two monomers are in close proximity. The move is performed by cutting the tail chain at the internal monomer and attaching it to the end of the neighboring chain [16,17]. Double bridging moves work by identifying two pairs of bonded monomers in spatial proximity. The move is performed by replacing the two intramolecular bonds by two intermolecular bonds to swap the tails of the two polymers. The result of these moves is a melt conformation with a new chemical connectivity. Compared with end-bridging moves double-bridging preserves the chain length when equivalent bead pairs along the polymer contours are chosen.

The double bridging moves are the best way currently known to accelerate the polymer dynamics in dense melts, but the method suffers from two major problems: (1) as the chain length is increased the density of potential sites for double bridging drops, and (2) the new proposed connectivity can have a high configurational energy, hence necessitating further tricks to relax the conformation to ensure a reasonable acceptance rate. For instance, it was proposed to reconnect not just monomers, but to grow small bridge segments in order to reduce the conformational energy of the proposed new state [15]. These methods have been used to equilibrate linear melts of polyethylene up to 1000 monomers [15,18], and polydisperse polyethylene melts up to 5000 monomers [19]. They have also been applied to branched molecules [20–22] and grafted polymers [23,24].

The first multiscale approach was introduced by Subramanian [25,26], who applied it to linear and branched melts. His idea was to start by equilibrating a coarse representation of the polymer, and successively rescale the simulation domain by while doubling the number of beads in the polymer model. In this way polymer conformations are successively equilibrated on smaller and smaller length scales. A more sophisticated version of hierarchical equilibration has been studied by Zhang *et al.* [27], where a range of blob chain models were successively fine grained with a force field that depended on the scale of fine graining. The most recently proposed equilibration method is that of Moreira *et al.* [28], who develop the Auhl method further by applying a warm-up procedure where pair interactions are slowly introduced via a cap on the maximal force as well as the cutoff distance of the pair interactions that is progressively raised using an elaborate feedback control mechanism during the equilibration process.

Equilibrated melts of atomistic polymer models can be obtained via fine-graining from a coarse-grained polymer model. Theodorou and Suter [29,30] studied polymer melts with atomistic models which they prepared by growing atomistic polymer models bond-by-bond in the simulation domain using a metropolis acceptance criterion while taking nonbonded interactions into account when choosing bond angles. The resulting states were then energy minimized. Carbone *et al.* [31] produce atomistic polymer melts by generating continuous (nonpacked) random walks and fine-graining them using an atomistic polymer models. For each continuous random walk, a corresponding atomistic polymer chain is created by confining the configuration to follow the continuous random walk, and intrachain monomeric packing is slowly introduced through a simulation with a soft push-off potential. In a second step, the atomistic polymer chains are placed in the simulation domain, and a second push-off procedure is performed to introduce interchain monomeric packing. A similar approach was used by Kotelyanskii *et al.* [32] but using self-avoiding random walks on a cubic lattice for the initial random walks, which resolves the packing problem. Recently, Sliozberg *et al.* [33] equilibrated a one million atom system of polyethylene using an united atom model. Similar to Theodorou and Suter the polymers are grown in the simulation domain, taking chemical structure into account to some extent. The resulting melt conformations are then simulated with a soft DPD inspired potential to gently introduce excluded volume interactions, until they can be switched to the final united-atom force field.

In the present paper, our aim is to present a general, simple, and computationally effective method of rapidly generating

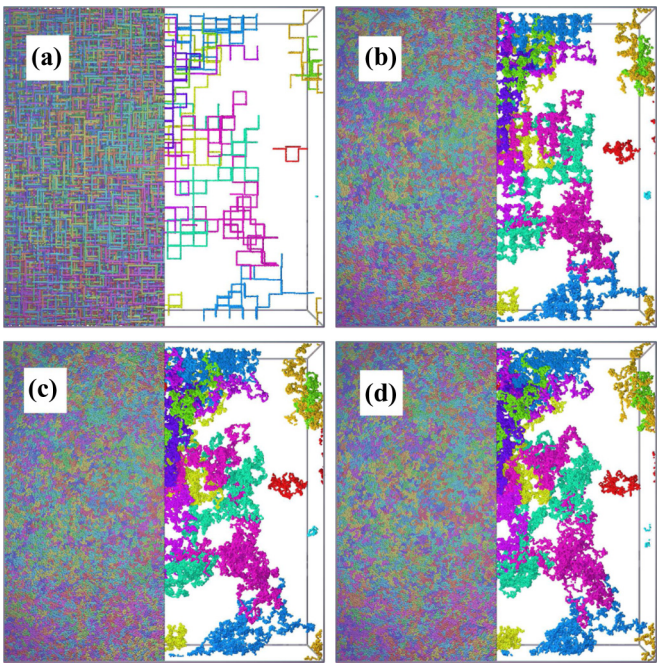


FIG. 1. Visualization of a melt of 1000 chains of 15 000 beads each during the equilibration process. All the polymers are shown on the left hand side of the box, while the same ten randomly selected polymers are shown on the right hand side of the box. Conformation just after lattice annealing (a), after $0.1\tau_e$ (b), and $1\tau_e$ (c) of Rouse dynamics simulation with the force-capped KG model, and final melt configuration after KG warmup (d).

very large equilibrated melts of polymers. We illustrate the method by creating equilibrated monodisperse linear Kremer-Grest (KG) [34] polymer models. This polymer model is the standard model for molecular dynamics simulations of polymers. The KG model is generic and describes universal polymer properties without attempting to model chemical details of specific polymer species. Chemical details can be introduced in the KG model by varying the effective chain stiffness, which allows us to use this model for studying universal properties of specific polymer types [35]. Here we study how to produce equilibrated melts for a wide range of chain stiffnesses. The typical size of the melts we generate in this study comprise $5–15\times10^6$ beads for chains of 15 000 beads per chain or 200 entanglements per chain. These numbers are chosen be about a factor of 5 above the state of the art, e.g., [27,28]. However, we are by no means pushing the limits of the present equilibration approach.

We borrow ideas from many of the approaches described above, but with a few twists and improvements, the most important being that we use different polymer models and methods at different scales just as Rosa *et al.* [36]. First we equilibrate the melt above the tube length scale. We model a polymer as a random walk of entanglement blobs on a cubic lattice and minimize density fluctuations using Monte Carlo simulated annealing [Fig. 1(a)]. The lattice melt conformation is transferred to a bead-spring melt conformation. Subsequently we equilibrate the chain structure inside the tube using a molecular dynamics simulation of a capped force field inspired from dissipative-particle dynamics [37,38]. We have designed this model to reproduce the chain statistics of the desired target KG model. The force-capped model produces Rouse dynamics, and after a short simulation we achieve the equilibrium local chain structure and entanglement density without reintroducing density fluctuations [Figs. 1(b) and 1(c)]. Finally we transfer the force-capped melt state to the KG force field and thermalize the conformations to produce the correct local bead packing [Fig. 1(d)].

Each of these stages are fast because we are using computationally efficient models at each scale. For the lattice annealing, we use a Hamiltonian that only depends on the local blob density, and hence is fast to evaluate. Furthermore, one of the moves we use is a double-bridge move. On a lattice candidate moves are easy to identify and they are always accepted which leads to fast equilibration dynamics. The lattice annealing is the only part of the our procedure that depends on the specific molecular structure. However, since the lattice melts are highly coarse-grained and we use effective moves, the computational effort required for the lattice annealing is trivial. In the second stage, the force cap allows chains to partially pass through each other, which accelerates the dynamics by reducing the effective bead friction. By retaining a weakly repulsive pair interaction we also ensure that density fluctuations continue to be annealed further during this stage. The largest computational effort goes into this stage, which is given by the entanglement time of the force-capped model. This is independent of the large scale molecular structure of the polymers, hence we can equilibrate an arbitrarily branched polymer melt in the same time as it takes to equilibrate a simple linear melt. The final thermalization with the target KG model is required to equilibrate the local bead structure and reduces density fluctuations even further; this only requires a brief simulation to allow beads to move a distance of the order of their own size.

The paper is structured as follows; In the short theory section we introduce the basic concepts and quantities characterizing polymer melts. In Sec. III, we define the three polymer models that we use in the paper, and characterize them to the extent required for transferring melt states between them. In Sec. IV, we proceed to characterize the equilibration process in terms of single-chain, collective, and bulk observables at microscopic, mesoscopic, and macroscopic scales. Finally, we conclude in Sec. V. In Appendix A we present the equilibration process in the form of an easy to follow recipe, and in Appendix B we derive some results for structure factors.

## II. CHARACTERISTICS OF POLYMER MELTS

Below we introduce the characteristic spatial and temporal scales associated with polymers conformations and their dynamics. At the molecular scale, we can characterize the single chain statistics in a polymer melt as a ideal random walk, since excluded volume interactions are approximately screened [39,40]. We can characterize chain statistics either in terms of number of carbon atoms in the backbone or number of monomers, however, since our target here is the KG bead-spring model, we express conformations in terms of the number of beads $N_b$ per chain. The end-to-end distance of a chain of $N_b$ beads is then given by

$$\langle R^2(N_b)\rangle = c_b l_b^2 N_b = l_K L_K, \tag{1}$$

where $l_b$ is the average bond length, and $c_b = l_K/l_b$ is the chain stiffness due to bead packing and local chain structure. For $N_b \gg 1$ the chain stiffness is given by $c_b = [\langle\cos\theta\rangle + 1]/[\langle\cos\theta\rangle - 1]$, where $\theta$ denotes the angle between subsequent bonds. At the Kuhn scale (denoted by subscript "$K$") the chain statistics becomes particular simple. It is described by a random walk with contour length $L_K = l_K N_K = l_b N_b$ where the walk consists of $N_K$ Kuhn segments that are statistically independent, i.e., $c_K = 1$ at and above the Kuhn scale.

The Kuhn length can be estimated using

$$l_K = \frac{\langle R^2(N_b)\rangle}{L_K} = 2\sqrt{\langle l_b^2\rangle}\int_0^{N_b}\left(1 - \frac{n}{N_b}\right)C(n)dn, \qquad (2)$$

where we have expressed the mean-square end-to-end distance in terms of the bond correlation function $C(n) = \langle \boldsymbol{b}(m)\cdot\boldsymbol{b}(m+n)\rangle_m$. This correlation function characterizes along how many bonds correlations between bond directions persists. The bond correlation function is easy to sample from simulations.

To define a mesoscopic length scale due to collective chain effects, we can look at the most characteristic macroscopic material property of a polymer melt—the plateau modulus. Since polymers cannot move through each other, thermal fluctuations are topologically constrained. This leads to a localization of the thermal fluctuations inside a tubelike shape of typical size $d_T$ [41]. Each topological entanglement contributes a free energy of $k_B T$, and the plateau modulus is the corresponding free energy density

$$G_N = \frac{4}{5}\frac{\rho_K kT}{N_{eK}}. \qquad (3)$$

Here $\rho_K = \rho_b/c_b$ is the number density of Kuhn segments, $\rho_b$ is the number density of beads, $k$ is the Boltzmann constant, and $T$ is the temperature. The entanglement length $N_{ek}$ is a measure of the contour length between topological entanglements along the chain. Note that we specify it in terms of Kuhn units and not beads between entanglements. In the present paper, we generally report results in terms of Kuhn units rather than numbers specific for the KG model. This is to simplify comparisons with theory and experiment, since in Kuhn units we would characterize a real chemical molecule and one of our model molecules with exactly the same numbers independent of the chosen polymer model. The 4/5 prefactor is due to the entanglements lost as the stretched chains initially retract into the tube to reestablish their equilibrium contour length [5].

We can relate the length of a tube segment $d_T$ to the number of Kuhn units it contains as $d_T^2 = l_K^2 N_{eK}$ and $Z = N_K/N_{eK}$ as the number of entanglements or tube segments per chain. Since the tube is a coarse representation of the chain it contains, the large scale tube and chain statistics must coincide, while below the tube length scale, the tube is straight and the chain performs a random walk. In particular, the chain end-to-end distance matches the end-to-end distance of the tube $\langle R^2\rangle = d_T^2 Z = l_K^2 N_K$.

The dynamics of short unentangled polymer melts, is described by the Rouse model [5,42], which also describes the local dynamics of long entangled melts. In this model, a chain is represented by a flexible string of noninteracting units connected by harmonic springs, i.e., each unit represents one Kuhn segment of the polymer. Besides the forces that arise due to connectivity, each unit also receives a stochastic kick and is affected by a friction force, i.e., the Rouse model is endowed with Langevin dynamics. The combined effects of these two forces are to model the presence of the other chains in the melt. The Rouse model can be solved exactly analytically by transforming it to a mode representation; see, e.g., [5]. In particular, the Rouse model predicts the chain center-of-mass diffusion coefficient $D_{cm}$ and its relation to the Kuhn friction $\zeta_K$ as

$$D_{cm} = \frac{kT}{\zeta_K N_K}, \qquad (4)$$

which has the form of a fluctuation-dissipation theorem. This relation can be inverted to derive the Kuhn friction from a measured diffusion coefficient. The fastest dynamics is that associated with the diffusive motion of individual Kuhn segments one Kuhn length, i.e., $\tau_K \sim l_K^2 D_K^{-1} \sim \zeta_K l_K^2/kT$. A more careful derivation provides the prefactor as

$$\tau_K = \frac{\zeta_K l_K^2}{3\pi^2 kT}. \qquad (5)$$

In the case of entangled melts, we can define the entanglement time which is the characteristic time it takes an entangled chain segment to diffuse the length of a tube segment $\tau_e \sim d_T^2(D_K/N_e)^{-1} \sim l_K^2 N_e^2 \zeta_K/kT$, and with the correct prefactor

$$\tau_e = \tau_K N_e^2 = \frac{\zeta_K}{3\pi^2 kT}\frac{d_T^4}{l_K^2}, \qquad (6)$$

the entanglement time is typically much larger than the fundamental Kuhn time. The conformational relaxation times due to reptation (linear polymers) or contour length fluctuations (star polymers) is again typically much larger than the entanglement time.

The Kuhn length is a microscopic single chain property, and the tube diameter is a collective mesoscale property that is typically associated with pairwise entanglements [43]. In order to characterize bulk large scale melt properties and in particular density fluctuations, we use the structure factor. The structure factor is defined as

$$S(\boldsymbol{q}) = (N_b M)^{-1}\left\langle\left|\sum_{j=1}^{M}\sum_{k=1}^{N_b}\exp(i\boldsymbol{q}\cdot\boldsymbol{R}_{jk})\right|^2\right\rangle, \qquad (7)$$

where $\boldsymbol{q}$ is the momentum transfer in the scattering process. $M$ denotes the number of polymers, and $\boldsymbol{R}_{jk}$ is the position of the $k$th bead in the $j$th polymer. We assume for notational simplicity that all polymers have the same number of beads. When performing simulations with periodic boundary conditions, we are limited to momentum transfers on the reciprocal lattice of the simulation box, i.e., $\boldsymbol{q}$ vectors of the form $\boldsymbol{q} = (2\pi n_x/L, 2\pi n_y/L, 2\pi n_z/L)$, where $L$ denote the box size. Since the melts are isotropic, we average and bin the structure factor based on the magnitude of the momentum transfer vector denoted $q = |\boldsymbol{q}|$. The structure factor for small $q$ values converges to $\lim_{q\to 0} S(q) = \chi_T \rho kT$ where $\chi_T$ is the isothermal compressibility of the melt. For a further discussion on density fluctuations and compressibility, we refer to the more detailed derivations in Appendix B.

## III. POLYMER MODELS

In the following, we define and characterize the three polymer models employed in the present study: We begin with the KG model (Sec. III A); we also introduce a force-capped variant of the KG model (fcKG) (Sec. III B), and finally we introduce a model where chains are modelled as a string of entanglement blobs on a lattice (Sec. III C). We also characterize the Kuhn length for both the KG and fcKG models (Sec. III D), the tube diameter for the KG model (Sec. III E), and finally the Kuhn friction of the fcKG model (Sec. III F). These relations are required to transfer melt conformations between the different polymer models, and to determine how long a Rouse simulation is required for the equilibration process.

### A. Kremer-Grest polymer model

The end goal of the present equilibration procedure is to produce an equilibrated KG model melt [34,44]. This is a generic bead-spring polymer model, where all beads interact via a Weeks-Chandler-Anderson (WCA) potential,

$$U_{\mathrm{WCA}} = 4\epsilon\left[\left(\frac{\sigma}{r}\right)^{-12} - \left(\frac{\sigma}{r}\right)^{-6} + \frac{1}{4}\right] \quad \text{for} \quad r < 2^{1/6}\sigma, \tag{8}$$

while springs are modeled by finite-elastic-nonextensible spring (FENE) potential,

$$U_{FENE} = -\frac{kR^2}{2}\ln\left[1 - \left(\frac{r}{R}\right)^2\right], \tag{9}$$

where we choose $\epsilon$ and $\sigma$ as the units of energy and distance respectively. The unit of time is $\tau = \sigma\sqrt{m_b/\epsilon}$ where $m_b$ denotes the mass of a bead. We add an additional bending interaction given by

$$U_{\mathrm{bend}}(\Theta) = \kappa\,(1 - \cos\Theta)\,. \tag{10}$$

The bending potential was introduced by Faller and Müller-Plathe [45–47]. The KG models are simulated using Langevin dynamics, which couples all beads to a thermostat, and allows long simulations at constant temperature to be performed with reasonable large time steps. The Langevin dynamics is given by the conservative force due pair and bond interactions, as well as a friction term and a stochastic force term:

$$m\frac{\partial^2 \boldsymbol{R}_n}{\partial t^2} = -\nabla_{\boldsymbol{R}_n} U - \Gamma\frac{\partial}{\partial t}\boldsymbol{R}_n + \boldsymbol{\xi}_n, \tag{11}$$

where the stochastic force obeys $\langle\boldsymbol{\xi}_n\rangle = 0$ and $\langle\boldsymbol{\xi}_n(t)\cdot\boldsymbol{\xi}_m(t')\rangle = 6kT\Gamma\delta(t-t')\delta_{nm}$. The standard choice of the FENE bonds are $R = 1.5\sigma$ and $k = 30\epsilon\sigma^{-2}$, which produce a bond length of $l_b = 0.965\sigma$ [25]. The number of beads per Kuhn unit is given by $c_b = l_K(\kappa)/l_b$. The standard value for the thermostat coupling is $\Gamma = 0.5m_b\tau^{-1}$. KG model melts are typically simulated with a bead density of $\rho_b = 0.85\sigma^{-3}$. We use a time step of $\Delta t = 0.01\tau$. For integrating the dynamics of of KG model, we utilize the Grønbech-Jensen/Farago Langevin integration algorithm [48,49] implemented in the Large Atomic Molecular Massively Parallel Simulator (LAMMPS) [50].

### B. Force-capped KG model

The KG model preserves topological entanglements via a kinetic barrier of about 75 kT for chain pairs to move through each other [51]. This is due to the strong repulsive pair interaction in combination with a strongly attractive bond potential that diverges when bonds are stretched towards the maximal distance $R$. Preserving topological entanglements is essential for reproducing the plateau modulus. The lattice melt configurations has the correct large scale chain statistics, but as we will show later, the density of entanglements is much too low, hence directly switching from a lattice configuration to a topology preserving KG polymer model would produce model melts with a wrong entanglement density. Hence we need a computationally effective model to introduce the correct random walk statistics inside the tube diameter, and hence produce the correct entanglement density before switching to the KG model.

The force-capped KG model (fcKG) should solve this problem by (1) performing a Rouse like dynamics to introduce local random walk chain statistics, (2) prevent the growth of density fluctuations, (3) avoid the numerical instabilities due to short pair distances or long bonds which can occur in the lattice melt state or during the Rouse dynamics of the fcKG model, and finally (4) approximate the ground state of the KG force field such that we can transfer fcKG melt states to the KG force field with a minimum of computational effort.

Inspired from dissipative particle dynamics [37,38] and a previous equilibration method [27,28], we apply a force cap to the WCA potential as follows:

$$U^{\mathrm{cap}}_{\mathrm{WCA}}(r) = \begin{cases} (r - r_c)\,\frac{dU_{\mathrm{WCA}}}{dr}\big|_{r=r_c} + U_{\mathrm{WCA}}(r_c) & r < r_c \\ U_{\mathrm{WCA}}(r) & \text{otherwise} \end{cases}. \tag{12}$$

The inner cutoff distance $r_c$ determines the potential at overlap. We choose $U^{\mathrm{cap}}_{\mathrm{WCA}}(r=0) = 5\epsilon$ which corresponds to an inner cutoff of $r_c = 0.9558\times 2^{1/6}\sigma$. For the bond potential, we choose a fourth degree Taylor expansion of the sum of the original WCA and FENE bond potentials around the equilibrium distance ($r_0 = 0.9609\sigma$). The resulting bond potential is

$$\begin{aligned} U_{\mathrm{bond}}(r) = {} & 20.2026\epsilon + 490.628\epsilon\sigma^{-2}(r - r_0)^2 \\ & - 2256.76\epsilon\sigma^{-3}(r - r_0)^3 + 9685.31\epsilon\sigma^{-4}(r - r_0)^4. \end{aligned} \tag{13}$$

Finally we retain the bending potential

$$U_{\mathrm{bend}}(\Theta) = \kappa_{fc}\,(1 - \cos\Theta)\,, \tag{14}$$

and simulate the fcKG model with exactly the same Langevin dynamics as the full KG model.

Figure 2 shows a comparison between the pair and bonded potentials of the KG and fcKG models. The figure also shows the height of the energy barrier of chains passing through each other as a function of the force cap expressed as a function of the pair potential at overlap $U^{\mathrm{cap}}_{\mathrm{WCA}}(r=0)$. The transition state is a planar configuration of two perpendicular chains, where two perpendicular bonds open up to allow one chain to pass through the other. Compared to the KG model, this force cap reduces this energy barrier from $75\epsilon$ down to $7.5\epsilon$.

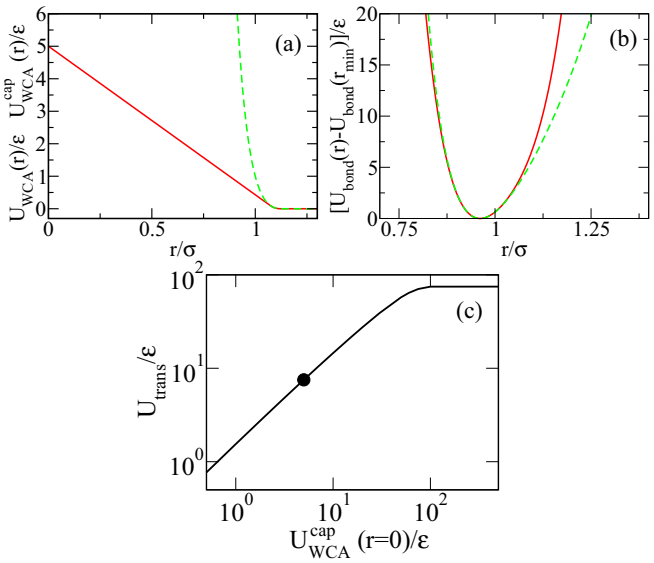


FIG. 2. The pair potential (a) and bond potential (b) for the full KG model (green dashed lines) and for the fcKG model (red solid lines). Shown is also the height of the energetic barrier for chains to pass through each other as function of the force cap (c). The circle denotes our choice of $U^{cap}_{WCA}(r=0)=5\epsilon$.

We avoid numerical instabilities by using the Taylor expansion in the fcKG model rather than FENE and WCA potentials between bonded beads in the KG model. As a result the numerical stability of the force-capped model is considerably improved both for very short and very long bonds. We can simulate the lattice melt states directly (after simple energy minimization) without requiring any elaborate push-off or warmup procedures to gradually change the force field. Since the force-capped model also approximates the ground state of the full KG model, we can also switch force-capped melt configurations to the full KG force field using simple energy minimization and also avoid designing a delicate push-off or warmup procedure for this change of force field. Furthermore, we expect an increased bead mobility while local single chain structure remains mostly unaffected. Note that in the KG model the WCA interaction is applied between all bead pairs, however for the fcKG model the WCA potential is already included in bond potential above, hence the force-capped pair interaction is limited to nonbonded beads.

### C. Lattice blob model

We coarse-grain space into a lattice on a length scale $a$ corresponding to the tube segment length $d_T$. The polymers become random walks on this lattice. Since multiple chains pervade an entanglement volume, multiple blobs can occupy the same lattice site. We regard the polymers as consisting of $Z$ entanglement blobs of $N_e$ Kuhn segments each. The number of chains within the volume associated with a blob is $n_e = \rho_K N_e^{-1} d_T^3$. For most flexible well-entangled polymers $n_e \sim 19$ [52].

We utilize the recently published lattice polymer model of Wang [53] which is based on a local term penalizing density fluctuations. This model has the computational advantage that the Hamiltonian does not include pair interactions, which makes it computationally very effective. We have augmented this Hamiltonian with an angle dependent term as follows:

$$H = \frac{1}{2\chi\langle n\rangle}\sum_c (n_c - \langle n\rangle)^2 + \sum_p (\epsilon_0 N_{p0} + \epsilon_{90} N_{p90} + \epsilon_{180} N_{p180}). \quad (15)$$

The first term is a sum over all sites, while the second is a sum over all polymers. $n_c$ denotes the blob occupation number at site $c$, while $\langle n\rangle \approx n_e$ is the average number of blobs per site. The parameter $\chi$ plays the role of a compressibility [54,55] and hence allows us to introduce incompressibility gradually to remove large scale density fluctuations. In the angle term we sum over bond angles in the chains. The three terms represents antiparallel, orthogonal, and parallel successive bonds and their respective energy penalties, respectively. The average bond-bond angle is in this case given by

$$\langle\cos\Theta\rangle = \frac{-\exp(-\beta\epsilon_0) + \exp(-\beta\epsilon_{180})}{\exp(-\beta\epsilon_0) + 4\exp(-\beta\epsilon_{90}) + \exp(-\beta\epsilon_{180})}; \quad (16)$$

to obtain a nonreversible random walk of blobs we require $\langle\cos\Theta\rangle = 0$, such that $c_L = [\langle\cos\theta\rangle + 1]/[\langle\cos\theta\rangle - 1] = 1$. We choose the parameters $\epsilon_0 = \epsilon_{180} = 1$ and $\epsilon_{90} = 0$. We furthermore choose $\chi = 1$. Since we are doing simulated annealing the exact values of these parameters are irrelevant. Any state with density fluctuations or configurations with deviations from nonreversible random walks will be exponentially unlikely when the temperature is reduced sufficiently.

We have implemented double bridging, pivot, reptation, and translate moves. Double bridge moves are performed by identifying two pairs of connected blobs on neighboring sites where "crossing over" the bond between the two pairs of blobs does not change monodispersity of the melt. Since double bridge moves alter neither angles nor blob positions, the double bridge moves do not change the energy, and are always accepted. Double bridge moves can be carried out both inside a chain and between pairs of chains. Pivot moves pick a random bond and randomly pivots the head or tail of the chain around the the chosen bond [56]. Pivot moves only change one angle at the pivot point, but cause major spatial reorganization of the polymer. In densely packed systems, the acceptance rate of pivot moves drops rapidly. Reptation moves delete a number of blobs at either the head or the tail of a polymer and regrows the same number of blobs at the other end of the polymer. Reptation moves are very efficient at generating new configurations in dense systems. Translate moves pick a random bond and randomize it, and hence randomly translates the head or the tail of the chain by one lattice step relative to the bond. Of the moves discussed here, only the reptation move is limited to linear chain connectivity. We implemented the Metropolis Monte Carlo algorithm in C++ (2011 standard version) making extensive use of standard-template library containers and pointer structures choosing optimal data structures for implementing the infrastructure for generating new moves, rejecting moves with a minimal overhead, and rapidly estimating the energy change of a given trial move [57].

We note that our choice of lattice length scale is in fact arbitrary, since the subsequent Rouse simulation with the fcKG

model removes the lattice artifacts again. From Eq. (6), we see that the Rouse simulation duration grows as the fourth power of the lattice constant. On the other hand, the advantage of enforcing the incompressibility constraint with a lattice Hamiltonian requires a meaningful site occupation numbers $n_c \gg 1$. When this limit is approached, the incompressibility constraint converges to an excluded volume constraint and blobs to single monomers. Matching the lattice spacing and the tube diameter produces $\langle n \rangle \sim 19$ which offers a reasonable compromise.

### D. Kuhn lengths of both KG models

In order to have the same chain statistics and in particular a specific Kuhn length for the force-capped and full KG models, we need to estimate how these change with stiffness. Theoretically predicting the Kuhn length of a polymer model with pair interactions is a highly nontrivial problem. While excluded volume interactions are approximately screened in melts (the Flory ideality hypothesis [39,40]), the melt deviates from polymers in $\Theta$ solutions due to their incompressibility. The incompressibility constraint creates a correlation hole, which leads to a long range net repulsive interaction between polymer blobs along the chain; this effectively causes a renormalization of the bead-bead stiffness to make them stiffer [58–62].

To circumvent this problem, we have brute force equilibrated medium length entangled melts with $M = 2000$ chains of length $N_b = 400$ beads while systematically varying the stiffness parameter for both the KG and fcKG models. Each initial melt conformation was simulated for at least $2\times10^5\tau$ while performing double-bridging hybrid MC-MD simulations [15,18,20,24] using the bond-swap fix in LAMMPS [63]. Ten to 20 configurations from the last $5\times10^4\tau$ of the trajectory were used to estimate the Kuhn length. We choose the chain length as a compromise between having as many Kuhn segments as possible and on having an acceptable double bridging acceptance rate. While double bridging moves are very efficient at removing correlations between the chain conformations, the acceptance rate drops significantly with chain lengths since the potential crossover points are progressively diluted when requiring that the melt remains monodisperse. The Kuhn lengths were derived using Eq. (2).

The resulting Kuhn lengths are shown in Fig. 3. As expected, as the stiffness parameter is increased the Kuhn length grows concomitantly. The stiffness of the fcKG and the KG models varies slightly. This is due to the additional stiffness introduced by the WCA pair interaction between next nearest neighbors along the chain compared to the force-capped model. Using the extrapolations shown in Fig. 3 we can numerically solve for the force-capped model stiffness $\kappa_{fc}$ required to reproduce equivalent KG model with stiffness parameter $\kappa$. The result is shown in the inset of Fig. 3, and is given by the following empirical relationship valid for $\kappa \in [-1\epsilon\colon 2.5\epsilon]$:

$$\kappa_{fc}(\kappa) = 0.298\epsilon + 0.722\kappa + 0.099\frac{\kappa^2}{\epsilon} - 0.012\frac{\kappa^3}{\epsilon^2}. \quad (17)$$

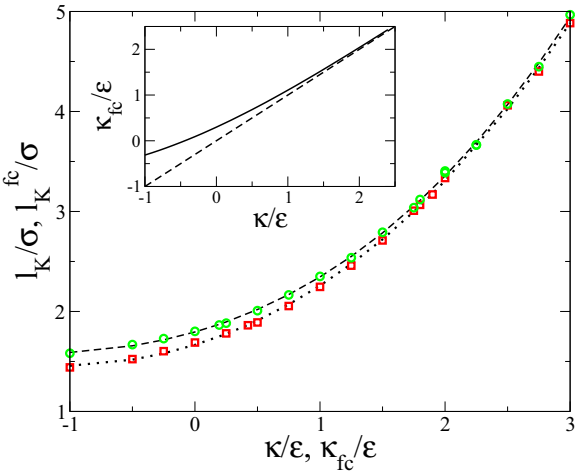


FIG. 3. Kuhn length $l_K$ vs stiffness parameter for the KG (green circles) and fcKG models (red boxes). The lines are polynomial fits $\frac{l_K(\kappa)}{\sigma} = 1.795 + 0.358\frac{\kappa}{\epsilon} + 0.172\frac{\kappa^2}{\epsilon^2} + 0.019\frac{\kappa^3}{\epsilon^3}$ (hashed black line) and $\frac{l_K^{fc}(\kappa_{fc})}{\sigma} = 1.666 + 0.389\frac{\kappa_{fc}}{\epsilon} + 0.192\frac{\kappa_{fc}^2}{\epsilon^2} + 0.012\frac{\kappa_{fc}^3}{\epsilon^3}$ (dotted black line). The inset shows the relation between $\kappa_{fc}$ and $\kappa$ defined by Eq. (17) (solid black line).

### E. Tube diameter of Kremer-Grest melts

In order to choose the spacing of the lattice model, we need to estimate the length of a tube segment $a(\kappa)$ as function of stiffness $\kappa$ for the KG model. We have generated 15 melt states with $M = 500$ chains of length $N_b = 10.000$ for $\kappa = -1, -0.75, -0.50, \ldots, 2.25, 2.50\epsilon$. We used the algorithm of the present paper, but chose the lattice spacing $a = l_K(\kappa)\sqrt{N_K(\kappa)}$, with $N_K(\kappa) = 100c_b^{-1}(\kappa)$. This corresponds to using not entanglement blobs, but rather blobs with a fixed number of beads (100) independently of chain stiffness.

We have performed primitive-path analysis (PPA) of the melt states [4]. During the PPA a melt conformation is converted into the topologically equivalent primitive-path mesh work characterizing the tube structure. We have performed a version of the PPA analysis which preserves self-entanglements by only disabling pair interactions between beads within a chemical distance of $2c_bN_{eK}$ bonds [51]. The minimization was performed using the steepest descent algorithm implemented in LAMMPS followed by dampened Langevin dynamics as described in Ref. [4]. The generated melts range from $Z(\kappa = -1\epsilon) = 80$ to $Z(\kappa = 2.5\epsilon) = 540$ entanglements per chain. Hence, these melts are strongly entangled, and we can neglect the effect of chain ends [64].

Since the large scale chain melt statistics and primitive-path statistics agree, the PPA essentially consists of filtering out the effects of thermal fluctuations on the chain configurations. The chain mean-square end-to-end distance is unchanged by the PPA, and hence the Kuhn length of the tube (the tube diameter) is given by $a = \langle R^2 \rangle / L_{pp}$. $L_{pp}$ is the average primitive-path contour length, which we obtain directly from the mesh work produced by the PPA. By preforming the analysis on melts of varying $\kappa$ we can obtain the tube Kuhn length as function of chain stiffness $a(\kappa)$. The result is shown in Fig. 4, and as expected, when the chains becomes stiffer they can pervade a large volume and hence become

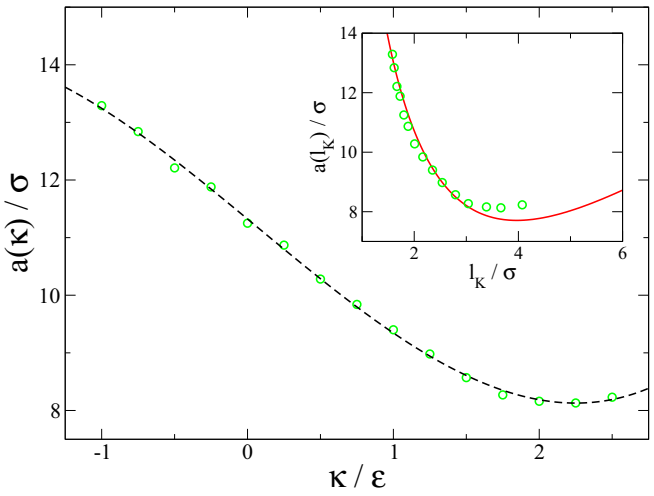


FIG. 4. Tube segmental length $a(\kappa)$ vs stiffness parameter for the KG model (green symbols); also shown is an interpolation given by $\frac{a(\kappa)}{\sigma} = 11.32 - 2.096\frac{\kappa}{\epsilon} - 0.0293\frac{\kappa^2}{\epsilon^2} + 0.1465\frac{\kappa^3}{\epsilon^3}$ (hashed line). The inset shows Eq. (18) (red solid curve) compared to the simulation data.

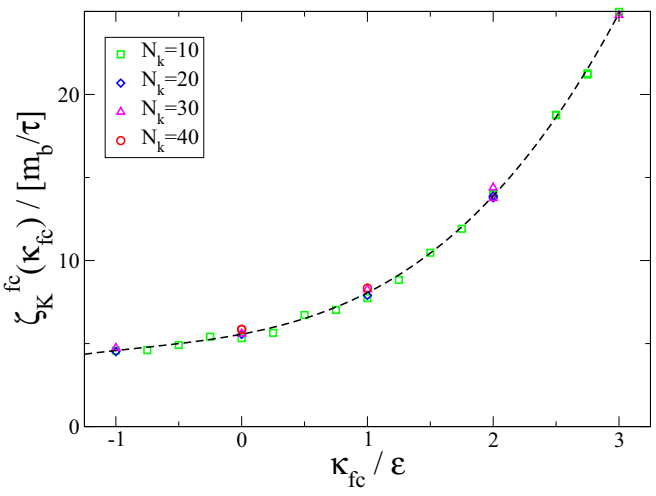


FIG. 5. Kuhn friction for the fcKG model as function of stiffness parameter $\kappa_{fc}$. The line through the data points is the fit $\frac{\zeta_K^{fc}(\kappa_{fc})\tau}{m_b} = 5.5657 + 1.4367\frac{\kappa_{fc}}{\epsilon} + 0.7564\frac{\kappa_{fc}^2}{\epsilon^2} + 0.303\,72\frac{\kappa_{fc}^3}{\epsilon^3}$.

more entangled, which corresponds to the observed decrease of the tube diameter. However in the limit of tightly packed rigid rods, the chain and tube Kuhn lengths coincide, hence the tube Kuhn length displays a minimum at the crossover from random walk to rigid rod chain behavior.

Combining Eqs. (2), (6), and (7) of Ref. [65], the tube Kuhn lengths dependence of the chain Kuhn length is predicted to be

$$a(l_K) = l_K\sqrt{1 + \left(c_\xi^2 l_K^6 \rho_K^2\right)^{-1} + \left(c_\xi^2 l_K^6 \rho_K^2\right)^{-1/5}}, \qquad (18)$$

where $c_\xi = 0.06$. This prediction is shown in the inset of Fig. 4 and is observed to be in very good agreement with our simulation data. The nonmonotonic behavior of $a$ as a function of $l_K$ is the expected signature of the crossover to the tightly entangled regime where $a = l_K$.

### F. Time mapping of the force-capped KG model

In order to estimate how long a time we should run the Rouse simulation to relax chain statistics up to the tube scale, we need to know the entanglement time of the fcKG model. The unit of time of the simulated force field is $\tau$, however, this unit has no direct relation to the time scales characterizing the emergent polymer dynamics, which depends on the force field as well as the thermostat parameters. To define a natural time scale for the polymer dynamics, we obtain the effective Kuhn friction $\zeta_K^{fc}$. We have measured the center-of-mass (CM) diffusion coefficient by performing a series of simulations with varying stiffness parameter $\kappa_{fc}$. Each melt contains 2000 chains of length $N_K = 10,20,30,40$. The melts were equilibrated for a period of $10^4\tau$ using double bridging hybrid MC-MD [15,18,20,24]. The resulting equilibrium states were run for up to $2 - 10 \times 10^5\tau$ and the center-of-mass diffusion coefficient $D_{cm}(\kappa_{fc}, N_K)$ was obtained from the plateau of the measured mean-square displacements $D_{cm}(\kappa_{fc}, N_K; t) = \langle[R_{cm}(t) - R_{cm}(0)]^2\rangle/[6t]$ for $t > 10^5\tau$ by sampling plateau values for log-equidistant times, and discarding simulations where the standard deviation of the samples exceeded 2% of their average value.

Figure 5 shows the Kuhn friction obtained from the analysis of the simulations using Eq. (4). We observe that the friction increases slowly with chain stiffness. The excellent collapse of data from different chain lengths supports the validity of the Rouse dynamics for the force-capped KG model.

Using Eq. (6) and the empirical relations shown in Figs. 3–5, we obtain an empirical relation for the entanglement time of the fcKG model as

$$\frac{\tau_e^{fc}(\kappa_{fc})}{\tau} = 935.5 - 710.8\frac{\kappa_{fc}}{\epsilon} + 226.6\frac{\kappa_{fc}^2}{\epsilon^2} - 26.61\frac{\kappa_{fc}^3}{\epsilon^3}, \qquad (19)$$

valid within the range of $\kappa_{fc} = -1, \ldots, 2.5\epsilon$. The entanglement time varies from $1900\tau$ down to $160\tau$ as chains get stiffer.

Figure 6 shows the mean-square displacements $\mathrm{MSD}(t) = \langle[\boldsymbol{R}_i(0) - \boldsymbol{R}_i(t)]^2\rangle$ of beads for the fcKG and KG models. We observe the expected subdiffusive Rouse power law $\mathrm{MSD}(t) \sim t^{1/2}$ for all times, whereas for the KG model we see the start of the crossover to a reptation dynamics $\mathrm{MSD}(t) \sim t^{1/4}$ power law above the entanglement time. The entanglement time depends on the entanglement length, and hence the stiffest chains reach the crossover first. These observations are consistent with our assumption that the fcKG model produces Rouse dynamics because it allows chains to pass through each other. Hence the entanglement Rouse time of the fcKG model is the relevant time for establishing local random walk structure inside the tube. The horizontal shift between the KG and fcKG models that the dynamics of the KG model is 6–7 slower than the fcKG model.

### G. Transferring melt states between models

Using the relations derived above we can fine-grain melt states from the lattice model to the fcKG model force field,

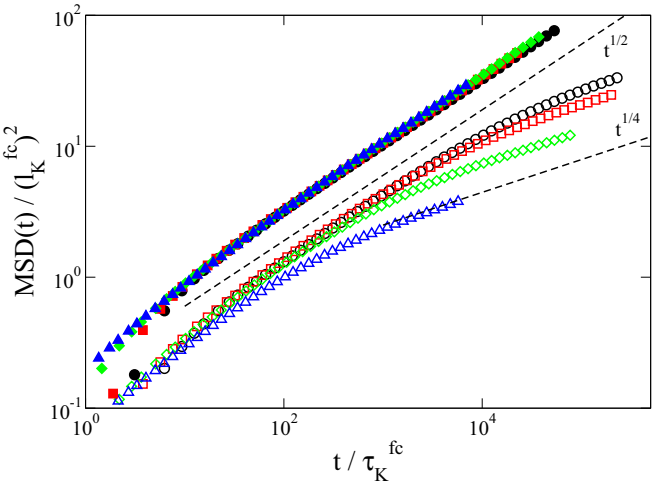


FIG. 6. Mean-square displacements for the fcKG model (filled symbols) and KG model (open symbols) for melts with $M \times N_b = 500 \times 10.000$ for $\kappa, \kappa_{fc} = -1\epsilon$ (black circle), $0\epsilon$ (red box), $1\epsilon$ (green diamond), and $2\epsilon$ (blue triangle up). The KG model data were scaled with the Kuhn length and time of the corresponding force-capped KG model to retain their relative positions.

and later transfer the fcKG melt states to the KG model force field and retain all the desired melt properties through the whole equilibration process. See Appendix A for the details.

## IV. CHARACTERIZATION OF EQUILIBRATION PROCESS

Figure 1 shows the evolution of a melt state with during the equilibration process. The melt comprises 1000 chains of 15 000 beads each, corresponding to $Z = 200$ entanglement blobs. Initially the lattice melt is density fluctuation annealed on a $23 \times 23 \times 23$ lattice. After lattice annealing of large scale density fluctuations, the final lattice polymer melt state is transferred to an off-lattice bead-spring model representation [Fig. 1(a)], that can be used as input for the subsequent molecular dynamics simulations. The subsequent Rouse simulation should introduce random chain structure at progressively larger and larger scales. After $0.1\tau_e^{fc}$ Rouse simulation [Fig. 1(b)] the lattice structure is still visible. However, after $1\tau_e^{fc}$ of Rouse simulation the polymers appears to have adopted a random walk conformation on the tube scale, and no signs of the lattice structure remain [Fig. 1(c)]. Transferring the resulting equilibrated fcKG melt state to the KG force field [Fig. 1(d)] does not affect the chain statistics. This final equilibrated melt state can then be used for further simulation studies.

Above, we characterized the KG and fcKG models using results for 15 melt states of $M \times N_b = 500 \times 10\,000$, i.e., $Z = 80, \ldots, 540$ entanglements for $\kappa = -1, -0.75, -0.50, \ldots, 2.25, 2.50\epsilon$. We have also equilibrated a number of large melts with $M \times N_b = 1000 \times 15\,000$, i.e., $Z = 200$ but only in the case of $\kappa = 0$. In comparison, the largest melts produced in Refs. [28,66] were 1000 chains of length 2000 beads. We produced eight melts using the full lattice Hamiltonian described above, five melts without the incompressibility term, and three melts without the configuration term. With these variations of the annealing procedure,

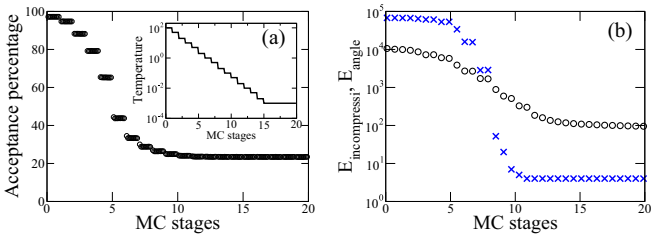


FIG. 7. Characterization of simulated annealing process showing (a) total acceptance probability and (b) the angle (blue crosses) and incompressibility (circles) energy contributions. The inset shows the temperature profile during annealing.

we can illustrate why both the incompressibility and angle terms are required. The lattice states were simulated with the same Rouse simulation, but we have also performed the KG warm up at different times during the Rouse simulation to study how this impacts the resulting KG melts. Below we will characterize the $1000 \times 15\,000$ melts states unless specifying a chain stiffness $\kappa$, in which case the observables are calculated for the $500 \times 10\,000$ melt states.

Figure 7 shows a characterization of the simulated annealing process. After some experimentation, we chose an annealing protocol where the temperature is reduced in 20 annealing stages from $T = 10^2$ to $10^{-3}$. At each annealing stage, we attempt 50 Monte Carlo (MC) moves per blob in the melt, where we use both global and local Monte Carlo moves. Above the transition temperature $T^* \sim 0.1$, the system rapidly equilibrates and the acceptance probability shows a clear step structure. Below the transition temperature, the equilibration slows down considerably and the steplike structure of the acceptance probability is lost. The acceptance rate remains clearly above 20% even below the transition temperature. This is primarily due to the end-bridging moves, which are attempted with 20% probability. The local chain dynamics becomes frozen while the global chain state remains dynamic, since double bridge moves are still accepted even below the transition temperature. Figure 7 also shows the decrease of the energy contributions from the incompressibility and angular terms in the lattice Hamiltonian. The angular energy contribution drops by about four orders of magnitude while the incompressibility energy drops by about two orders of magnitude. Both contributions level out after 10–12 annealing stages. After this time, the melt has reached its energy minimum.

Figure 8 shows the evolution of the chain conformations during the annealing process. We describe the large scale properties with the ratio of the end-to-end distance and the radius of gyration which for a random walk should be about 6 [40]. We observe that at large scales the melt conformations remain random walk like during the whole annealing process. Furthermore the scatter of the curves below the transition temperature again shows that the MC moves keeps generating new conformations searching for a better minimum.

The chain stiffness $c_L$ characterizes blob chain angle statistics at the tube scale. This should be unity for random walks where subsequent steps are statistically uncorrelated. For melts with the angular term, this is seen to be the case after some transients around the transition temperature, however, we see a slight but systematic increase in the chain stiffness for

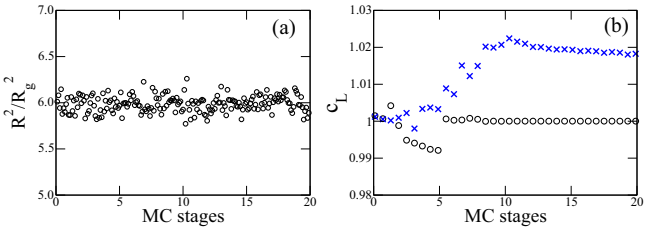


FIG. 8. Melt characterization during simulated annealing showing (a) $\langle R^2\rangle/\langle R_g^2\rangle \approx 6$ ratio and (b) chain stiffness $c_L$ for a lattice melt with (black circles) and without the angular energy contribution in the Hamiltonian (blue crosses).

melts without the angular term. This could be either due to the incompressibility constraint acting as a weak excluded volume even at occupation numbers of $\langle n\rangle \approx 19$, and hence leading to a small degree of swelling. Alternatively, it is also known that the Flory ideality hypothesis is only approximately true even for dense melts. The incompressibility constraint leads to a correlation hole of density fluctuations, which has been shown to give rise to an effective weakly repulsive intramolecular interaction [58–62]. Both these effects lead to swelling, and the severity of the swelling is likely to depend on the rate at which the simulated annealing process is quenched. We have opted for adding the additional angular term to the lattice Hamiltonian, to ensure that the lattice conformations show the desired random walk statistics.

Figure 9 shows the impact of incompressibility on the lattice melt conformations. At the lowest $q$ values, the structure factor characterizes density fluctuations on the scale of the whole simulation domain, whereas the highest $q$ values reflect density fluctuations on the scale of individual blobs. The structure factors were calculated for MD bead-spring melt states and include effects due to random shifts of chains and beads described above.

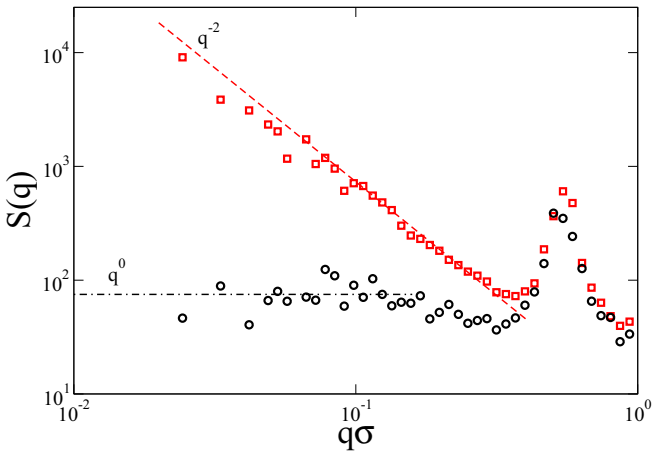


FIG. 9. Structure factor for initial lattice configurations with density fluctuations (red boxes), and after simulated annealing with the incompressibility term (black circles) averaged over several melt states. Also shown are the power laws expected from the density fluctuations and from incompressibility (red hashed and black dash-dotted lines, respectively).

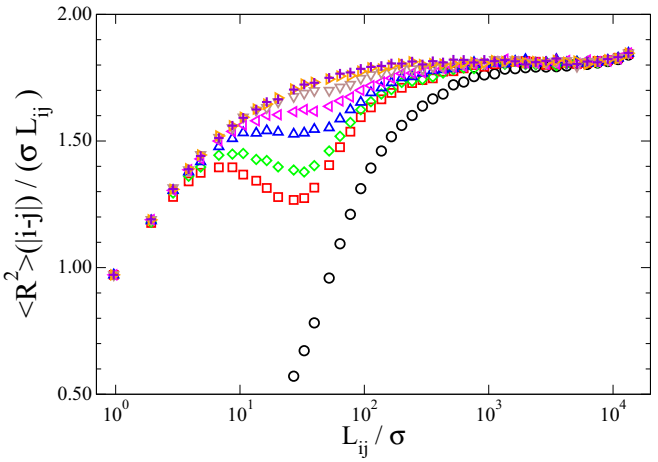


FIG. 10. Evolution of mean-square internal distances during equilibration for the initial lattice configuration (black circle), and after 0.1, 0.2,0.5,1, 2, 5, and $10\tau_e^{fc}$ (red box, green diamond, blue triangle up, red triangle left, brown triangle down, orange triangle right, purple plus, respectively) of Rouse simulation for $\kappa = 0$.

For the lattice simulations without the incompressibility term, very large scale density fluctuations can be seen at large scales, which follows the predicted power law behavior $S(q) \sim 2N_b(qR_g)^{-2}$, Eq. (B9). This power law reflects the density fluctuations created by randomly inserting the polymer chains on the lattice. After annealing, with the incompressibility term in the Hamiltonian the large scale density fluctuations are reduced by about two orders of magnitude, and the resulting structure factor is flat indicating constant density on all scales as expected for an incompressible melt. A large peak is seen in both the lattice configurations; this peak reflects the lattice structure and the position is given by $q_{\text{lattice}} = 2\pi/a$.

Figure 10 shows the evolution of single chain conformations characterized by their mean-square internal distances (MSID), which are defined by $\text{MSID}(L_{ij}) = \langle(\boldsymbol{R}_i - \boldsymbol{R}_j)^2\rangle/L_{ij}$ where $\boldsymbol{R}_i$ is the position of the $i$th bead on a chain, and $L_{ij} = l_b|i-j|$ denotes the chemical contour length between the two beads. For large chemical distances the MSID converges to the Kuhn length, whereas for neighboring monomers it is identical to the bond length $l_b$. Between these limits it characterizes the local effects of the chain stiffness.

The evolution of the chain statistics during the Rouse simulation is shown in Fig. 10. The final state from the lattice simulation matches the large scale chain statistics by construction, but shows strong compression at all length scales below the tube diameter, which is an expected lattice artifact. After energy minimization and a brief simulation, the bond distance agrees with the KG model, but chains are stretched at very short scales, and compressed at scales all the way to the tube scale. During the Rouse simulation, the chain statistics is progressively equilibrated at intermediate scales such that the desired chain statistics is established on all length scales. In the initial lattice configuration all the beads are compressed to a straight line and hence we approach the equilibrium chain statistics from below, whereas in the approach of Auhl *et al.* [12], their push off produced a peak in the MSID that is

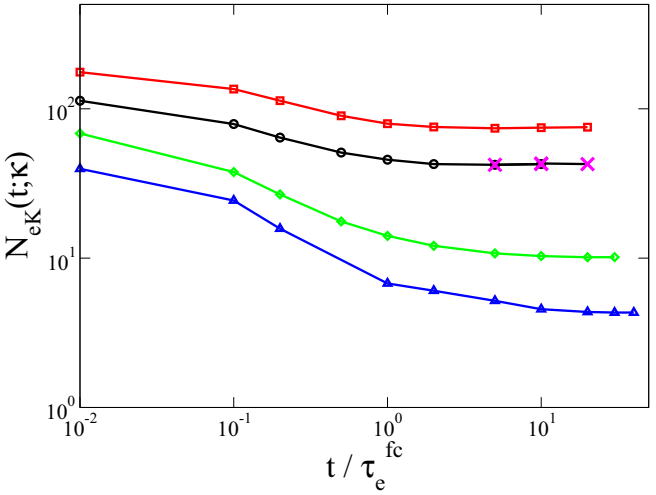


FIG. 11. Topological evolution of the melt during the Rouse simulation. The entanglement lengths of the force-capped KG model melts for $\kappa = -1\epsilon$, $0\epsilon$, $1.5\epsilon$, and $2.5\epsilon$ (denoted by red box, black circle, green diamond, and blue triangle up, respectively). Also shown are the entanglement length of melts after the KG warm up for three different times along the Rouse simulation for $\kappa = 0\epsilon$ (magenta crosses).

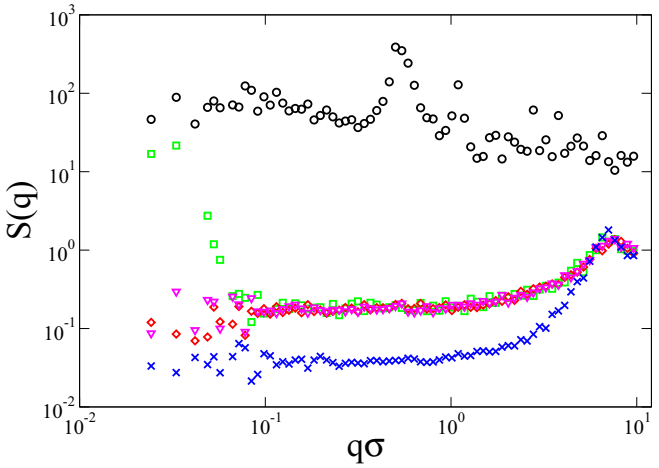


FIG. 12. Evolution of structure factor during equilibration process. Structure factor for the annealed lattice (black circle), after 0.1, 1, and $10\tau_e^{fc}$ (denoted by green box, red diamond, and magenta triangle up, respectively) of Rouse simulation, and for the final melt state after KG warm (blue cross).

due to local chain stretching due to density fluctuations, which was mitigated by the introduction of a prepacking procedure. Here our fcKG model has been designed to perform this prepacking on scales below the tube diameter during the Rouse simulation. The same behavior is observed for the other chain stiffness (data not shown).

The MSID is a single chain observable; we can also take melt configurations at various times along the Rouse dynamics simulation and submit them to PPA analysis to estimate the topological evolution of the melt. The entanglement length has been shown to be quite sensitive to the equilibration procedure, since chain stretching during equilibration of badly prepared samples artificially increases the entanglement density [67]. The result is shown in Fig. 11. The entanglement length is seen to systematically decrease towards the equilibrium entanglement length after about one entanglement time of Rouse dynamics independently of chain stiffness. During the Rouse simulation chains can pass through each other, however, during the PPA the topological structure is frozen. Hence the figure shows the growth of the entanglement density due to the random chain structure that is gradually introduced by the Rouse dynamics of the fcKG model. The figure also shows that the initial lattice states produce a completely wrong entanglement density, hence any attempt to equilibrate it with a topology preserving chain model would fail. Also shown are the entanglement lengths of the three melt conformations after the KG warm, which are seen to be in excellent agreement with the fcKG melt conformations. As expected the KG warm up does not change the topological melt structure.

The structure factor during the Rouse simulation and after the KG warm up is shown in Fig. 12. The structure factor measures density fluctuations and when constant allows us to estimate the compressibility of the melt (for the derivation see Appendix B). We see that the melt compressibility rapidly decreases by about three orders of magnitude when lattice melt states are equilibrated with the fcKG model. Residual density fluctuations are still observable at $0.1\tau_e^{fc}$ at large scales, but after $1\tau_e^{fc}$ density fluctuations are absent on all scales. After the KG warmup, the compressibility is further reduced by about one order of magnitude on all scales. The peak at $2\pi/a$ is gone, and a new peak is visible at $2\pi/\sigma$ which is due to local liquid like bead packing. The structure factors for melts with varying stiffness show similar behavior (data not shown).

Figure 13 compares the MSID for different stiffness of rapidly equilibrated long melts and brute force equilibrated shorter melts used to estimate the Kuhn lengths. The Rouse simulations were performed for $10\tau_e^{fc}$ when $\kappa < 1.5\epsilon$, $20\tau_e^{fc}$ for $\kappa = 1.5\epsilon$, $30\tau_e^{fc}$ for $\kappa = 2.0\epsilon$, and $40\tau_e^{fc}$ for $\kappa = 2.5\epsilon$. The entanglement time drops rapidly with increasing chain

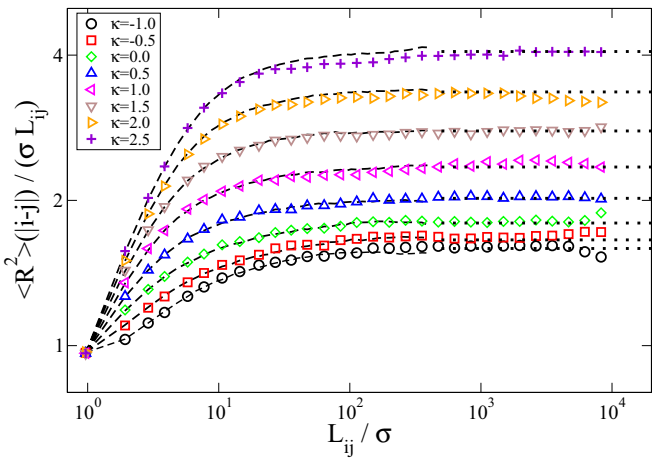


FIG. 13. Mean-square internal distances of equilibrated melts (colored symbols) compared to brute force equilibrated melts (dashed black lines) and Kuhn length (dotted black line) for varying stiffness.

stiffness, hence the highest computational effort is actually expended in equilibrating the most flexible melt with $\kappa = -1\epsilon$, which requires about a factor of 3 longer simulation time than the stiffest melts despite these running for five entanglement times longer.

The chain statistics shown in Fig. 13 are in good agreement with the brute force equilibrated melts at short scales; furthermore all the melts levels off to the expected plateau given by the Kuhn length at large scales. A small dip is seen for the two stiffest melts shown in the figure for an intermediate length scale $L_{ij} \approx 100$. Perhaps the stiffest melts are locally nematically ordered, in which case the energy barrier for chain interpenetration could be larger than expected and hence explain why we apparently need to run the simulation for longer than expected from Rouse dynamics. Clearly, the MSID is the measure that is the slowest to converge to the equilibrium since the bulk properties and collective mesoscopic properties measured by the structure factor and melt entanglement length have already reached their equilibrium values after about $1\tau_e$. Hence we suggest to use this observable as the main diagnostic for testing whether equilibrium has been achieved.

## V. CONCLUSIONS

We have shown how to equilibrate huge model polymer melts in three simple stages for Kremer-Grest polymer melts [34] of varying chain stiffness. First, density fluctuations are annealed on scales above the tube scale using Monte Carlo simulated annealing with a lattice polymer model. Second, with a molecular dynamics simulation of a force-capped KG (fcKG) polymer model, we simulate the Rouse dynamics [42] and introduce the desired chain structure on scales below that of the tube while preventing the growth of density fluctuations. Finally, we perform a fast warmup to the KG force field to establish the correct local bead packing. We have characterized the involved models for varying chain stiffnesses in order to transfer melt states between them. By measuring the Rouse friction of the fcKG model, we have also estimated the simulation time required for the equilibration of chain structure inside the tube, which was shown to be strongly dependent on chain stiffness.

We have also characterized and validated the equilibration process in terms of (1) single chain observables such as mean-square internal distances, (2) collective mesoscopic melt properties such as the evolution of the entanglement length during the Rouse dynamics, and (3) bulk melt density fluctuations in terms of structure factors. We have demonstrated the convergence of these observables to their equilibrium values for varying chain stiffnesses.

The main requirement of an equilibration process is computational performance. Here we have equilibrated 15 melts of 500 chains with 10 000 beads each for varying stiffness, and several melts of 1000 chains of 15 000 beads each for varying lattice annealing parameters. For the latter melts, the lattice annealing of density fluctuations takes about 3 days computer time using a single core on a standard laptop (72 core hours). Rouse simulation with the fcKG model for $10\tau_e$ takes about 2 days on 4 ABACUS2 nodes [68], i.e., 4600 core hours of compute time. Finally introducing the full KG model, requires about 2 h on four nodes, i.e., 200 core hours. Moreira [28] equilibrated $1000\times2000$ melts using 3500 core hours for prepacking (equivalent to our lattice annealing), and 3800 core hours for subsequent warmup. Zhang *et al.* [27] equilibrated similar sized melts but using a multiscale method that required 1600 core hours. Scaling these numbers to a standard melt of one million beads, the method of Moreira *et al.* would require 3600 core hours, the method of Zhang *et al.* would requires 800 core hours, while our method would require 600 core hours. This could be further optimized; e.g., the choice of the force cap is entirely serendipitous, and we use the standard values of the KG polymer model, which could be optimized further.

The present method is essentially independent of, e.g., chain length and the large scale polymer structure such as branching. These only impact the lattice annealing stage of the equilibration procedure, which due to the high level of coarse-graining is the fastest part of the equilibration process. The Rouse simulation and KG warmup are completely independent of the chain structure and composition. Hence the present method can directly be used to equilibrate, e.g., polymer melts of stars or mixtures of different polymer structures. Furthermore, the equilibrated KG melt configurations produced by the present approach can be fine-grained further to act as starting points for atomistic simulations of polymer melts.

With simple and computationally efficient equilibration approaches such as the one presented here, access to well equilibrated melts for studies of material properties is no longer a computational limitation, rather the computational limitation becomes the effort required to perform scientific studies using such huge systems.

## ACKNOWLEDGMENTS

R.E. would like to acknowledge stimulating discussions with A. Rosa. Computation and simulation for the work described in this paper were supported by the DeiC National HPC Center at University of Southern Denmark.

## APPENDIX A: EQUILIBRATION PROCESS

Below we summarize the equilibration process in the form of an easy to follow recipe. Assume we should generate a melt $M$ chain of $N_k$ Kuhn units each for chain stiffness $\kappa$. Alternatively if we should make chains of $N_b$ beads then $N_k = N_b/c_b$. Here $c_b = l_K/l_b$ beads per Kuhn length using the expression from Fig. 3. Here and below we suppress the dependency of $c_b, l_k, a, N_{eK}$ on stiffness for the sake of brevity.

First we set up the lattice melt. The lattice constant $a$ is determined using the interpolation Fig. 4. The number of entanglement blobs is $Z = \text{round}(N_k/N_{eK})$ with Kuhn entanglement number $N_{eK} = a^2/l_K^2$. The total number of beads in the melt is $N_b^{\text{tot}} = c_b N_{eK} Z M$ and the volume of the cubic lattice is $V = N_b^{\text{tot}}/\rho_b = (aN_s)^3$ where $N_s^3$ is the total number of lattice cells. The number of lattice sites $N_s^3$ is determined by $N_s = \text{round}([N_b^{\text{tot}}/\rho_b]^{1/3}/a)$.

Since the KG model is sensitive to deviations from the standard bead density, we correct for the round off errors due to integer $Z$ and $N_s$ values by self-consistently determining

the number of molecules as $M = \text{round}(\rho_b a^3 N_s^3/[c_b N_{eK} Z])$ that produce the standard bead density. The resulting lattice melt is generated and annealed as described in Sec. III C to ensure a homogeneous melt of entanglement blobs.

The next step is to transfer the lattice melt state to a MD melt conformation. Let the configuration of a single chain be described by integer coordinate vectors $\boldsymbol{R}_i$ for $i = 1, \ldots, Z$. The corresponding off-lattice chain is given by the scaled coordinates $a(\boldsymbol{R}_i + \boldsymbol{\xi})$ where $\boldsymbol{\xi}$ is a uniformly distributed random vector in $[-0.5 : 0.5]^3$. This chain defines a piecewise linear curve with contour length $aZ$. To obtain a MD chain configuration the curve is decorated with $c_b N_e Z$ beads corresponding to a bead contour length density of $c_b N_e/a$. A small random shift from a randomly sampled vector in $[-a/200, a/200]^3$ are furthermore added to each bead to facilitate energy minimization.

To perform the Rouse dynamics with the force-capped KG model, we first obtain the fcKG model stiffness $\kappa_{fc}$ using Eq. (17) with the specified target $\kappa$. The lattice configuration is then energy minimized with respect to the fcKG force field, and is then run with this force field for 10–40$\tau_e^{fc}$ depending on the stiffness. The fcKG model entanglement time $\tau_e^{fc}$ is obtained using Eq. (19).

During the Rouse dynamics simulation the structure factor, mean-square internal distances, and entanglement length of the melt conformations is monitored to ensure that they converge to an equilibrium. The resulting fcKG melt conformation has the correct chain statistics, entanglement density, and no density fluctuations

The final step is to transfer the fcKG melt state to the KG force field and thermalize it. This is done by first replacing the force-capped pair interaction with the full WCA interaction and minimizing the energy while keeping the fcKG bond potential; subsequently this bond potential is replaced by the WCA + FENE potential of the KG model and again energy minimized. Finally the resulting melt state is thermalized to introduce the correct local bead packing by a short simulation of $5\times10^4$ MD steps at $T = 1\epsilon$ with the full KG force field. The result is an equilibrated KG melt state that can be used for subsequent scientific studies.

## APPENDIX B: STRUCTURE FACTORS

Below we derive predictions for the structure factor due to the density fluctuations created by randomly inserting polymers in the simulation box, and the structure factor after equilibration of density fluctuations and its relation to the compressibility.

We define the microscopic density field $\rho(\boldsymbol{R}) = \sum_{j=1}^{M}\sum_{k=1}^{N}\delta(\boldsymbol{R} - \boldsymbol{R}_{jk})$, where $\delta$ denotes the Dirac-$\delta$ function. The Fourier transform of the density field is $\rho(\boldsymbol{q}) = \sum_{j=1}^{M}\sum_{k=1}^{N_b}\exp(i\boldsymbol{q}\cdot\boldsymbol{R}_{jk})$, such that the structure factor becomes

$$S(q) = (N_b M)^{-1}\langle\rho(-\boldsymbol{q})\rho(\boldsymbol{q})\rangle. \tag{B1}$$

To derive the structure factor after equilibration of density fluctuation, we start by expressing the structure factor in terms of spatially varying densities. From the right hand side of Eq. (B1) we get

$$\begin{aligned} S(\boldsymbol{q}) &= \left\langle \int d\boldsymbol{R}_1 d\boldsymbol{R}_2 \rho(\boldsymbol{R}_1)\rho(\boldsymbol{R}_2)\exp[i\boldsymbol{q}\cdot(\boldsymbol{R}_1 - \boldsymbol{R}_2)]\right\rangle \\ &= \int d\boldsymbol{R}_1 d\boldsymbol{R}_2 \exp[i\boldsymbol{q}\cdot(\boldsymbol{R}_1 - \boldsymbol{R}_2)]\,\langle\delta\rho(\boldsymbol{R}_1)\delta\rho(\boldsymbol{R}_2)\rangle \\ &= \int d\boldsymbol{R}\exp(i\boldsymbol{q}\cdot\boldsymbol{R})\,\langle\delta\rho(0)\delta\rho(\boldsymbol{R})\rangle\,, \end{aligned} \tag{B2}$$

where in the second equation we have replaced $\rho(\boldsymbol{R}) \to \delta\rho(\boldsymbol{R}) = \rho(\boldsymbol{R}) - \langle\rho\rangle$. The constant average density gives rise to a contribution proportional to a Dirac-$\delta$ function, which can be neglected for $q > 0$. In the third equation, we have furthermore assumed translational invariance.

Let us assume a local Hamiltonian for density fluctuations $H(\delta\rho) = \frac{1}{2\chi\langle\rho\rangle}\delta\rho^2$ for a particular position analogous to a site in the lattice model. The Boltzmann probability of a given density fluctuation is given by $P(\delta\rho) \propto \exp(-H/kT)$, and hence $\langle\delta\rho^2\rangle = \chi\langle\rho\rangle kT$ by the equipartition theorem. Assuming that the density fluctuations at different sites are statistically independent, which in practice is valid for sufficiently large distances, i.e., small values of $q$. The density fluctuation correlation function is then given by $\langle\delta\rho(0)\delta\rho(\boldsymbol{R})\rangle = \chi\langle\rho\rangle kT\,\delta(\boldsymbol{R})$. Inserting this in Eq. (B2), we obtain the prediction that the structure factor is independent of $q$ and proportional to the compressibility

$$S(q) = \chi\langle\rho\rangle kT. \tag{B3}$$

We can also predict the structure factor for polymers randomly inserted into the simulation domain using the approach in Refs. [69,70]. By introducing an origin of the coordinate system for each polymer $\boldsymbol{R}_j^o$, e.g., one of its ends, we can rewrite Eq. (7) as

$$\begin{aligned} S(q) = (N_b M)^{-1}\sum_{k_1=1}^{N_b}\sum_{k_2=1}^{N_b}\Bigg[\sum_{j=1}^{M}\left\langle\exp\left[i\boldsymbol{q}\cdot\left(\boldsymbol{R}_{jk_1} - \boldsymbol{R}_{jk_2}\right)\right]\right\rangle \\ + \sum_{\substack{j_1,j_2=1\\ j_1\neq j_2}}^{M}\Big\langle\exp\Big\{i\boldsymbol{q}\cdot\Big[\left(\boldsymbol{R}_{j_1k_1} - \boldsymbol{R}_{j_1}^o\right) - \left(\boldsymbol{R}_{j_2k_2} - \boldsymbol{R}_{j_2}^o\right) \\ + \left(\boldsymbol{R}_{j_1}^o - \boldsymbol{R}_{j_2}^o\right)\Big]\Big\}\Big\rangle\Bigg]; \end{aligned} \tag{B4}$$

here the first term describes the single polymer scattering due to pairs of scattering sites on the same polymer, while the second term is the interference contribution between scattering sites on different polymers. Configurations of different polymers are generated independently of each other, and the starting points of the polymers are chosen randomly. Hence the three terms in parentheses in the second exponential are sampled from statistically independent distributions. Having noted this, the average of the interference contribution factorize exactly into a product of three averages, where the first and third only depend on single chain statistics, while the second term only depends on the distance distribution between

randomly chosen points:

$$\left\langle \exp\left[i\boldsymbol{q}\cdot\left(\boldsymbol{R}_{j_1k_1}-\boldsymbol{R}^o_{j_1}\right)\right]\right\rangle_{j_1,k} \times\left\langle \exp\left[i\boldsymbol{q}\cdot\left(\boldsymbol{R}^o_{j_1}-\boldsymbol{R}^o_{j_2}\right)\right]\right\rangle_{j_1,j_2} \times\left\langle \exp\left[-i\boldsymbol{q}\cdot\left(\boldsymbol{R}_{j_2k_2}-\boldsymbol{R}^o_{j_2}\right)\right]\right\rangle_{j_2,k_2}. \tag{B5}$$

For notational simplicity, we can identify the average form factor as $F(\boldsymbol{q})=\left\langle \exp\left[i\boldsymbol{q}\cdot\left(\boldsymbol{R}_{jk_1}-\boldsymbol{R}_{jk_2}\right)\right]\right\rangle_{j,k_1,k_2}$ with the average single polymer scattering, $A(\boldsymbol{q})=\left\langle \exp\left[i\boldsymbol{q}\cdot\left(\boldsymbol{R}_{jk_1}-\boldsymbol{R}^o_{j}\right)\right]\right\rangle_{j,k_1}$ with the average form factor amplitude relative to an end, and the average phase factor between different ends $\Psi(\boldsymbol{q})=\left\langle \exp\left\{i\boldsymbol{q}\cdot\left[\left(\boldsymbol{R}^o_{j_1}-\boldsymbol{R}^o_{j_2}\right)\right]\right\}\right\rangle_{j_1\neq j_2}$. Note that all these factors are normalized as $F(\boldsymbol{q})=A(\boldsymbol{q})=\Psi(\boldsymbol{q})\to 1$ for $\boldsymbol{q}\to 0$. With these simplifications, the structure factor reduces to the much shorter expression

$$S(\boldsymbol{q})=N_bF(\boldsymbol{q})+(M-1)N_bA(\boldsymbol{q})\Psi(\boldsymbol{q})A(-\boldsymbol{q}). \tag{B6}$$

This expression is exact and was derived without any assumptions as to the detailed structure of the objects inserted in the simulation domain and only results from the assumption of statistical independence of internal conformations and positions of the objects [69]. For polymers modeled as ideal random walks, the expressions for the form factor and form factor amplitude are well known [71,72]:

$$F(q)=\frac{2\left[\exp\left(-q^2R_g^2\right)-1+q^2R_g^2\right]}{q^4R_g^4}\sim\frac{2}{q^2R_g^2}, \tag{B7}$$

$$A(q)=\frac{1-\exp\left(-q^2R_g^2\right)}{q^2R_g^2}\sim\frac{1}{q^2R_g^2}; \tag{B8}$$

since random walks on average are isotropic, these functions only depend on the magnitude of the scattering vector $q=|\boldsymbol{q}|$. The asymptotic behavior is realized for $qR_g\gg 1$, where $R_g=l_K^2N_K/6$ is the radius of gyration of the polymer. Furthermore, because polymers pairs are placed randomly in the box their starting positions are statistically independent, hence $\Psi(\boldsymbol{q})=1$. Hence for randomly inserted polymers, the asymptotic behavior of the structure factor describing the resulting density fluctuation correlations is

$$S(q)\sim\frac{2N_b}{q^2R_g^2}. \tag{B9}$$


[1] F. Snijkers, R. Pasquino, P. Olmsted, and D. Vlassopoulos, J. Phys.: Condens. Matter. **27**, 473002 (2015).
[2] J. Padding and W. Briels, J. Phys.: Condens. Matter **23**, 233101 (2011).
[3] Y. Li, B. C. Abberton, M. Kröger, and W. K. Liu, Polymers **5**, 751 (2013).
[4] R. Everaers, S. K. Sukumaran, G. S. Grest, C. Svaneborg, A. Sivasubramanian, and K. Kremer, Science **303**, 823 (2004).
[5] M. Doi and S. F. Edwards, *The Theory of Polymer Dynamics* (Clarendon, Oxford, 1986).
[6] P.-G. de Gennes, J. Chem. Phys. **55**, 572 (1971).
[7] P.-G. de Gennes, Macromolecules **9**, 587 (1976).
[8] J. Klein, Nature (London) **271**, 143 (1978).
[9] M. Zamponi, M. Monkenbusch, L. Willner, A. Wischnewski, B. Farago, and D. Richter, Europhys. Lett. **72**, 1039 (2005).
[10] D. S. Pearson and E. Helfand, Macromolecules **17**, 888 (1984).
[11] D. Brown, J. H. R. Clarke, M. Okuda, and T. Yamazaki, J. Chem. Phys. **100**, 6011 (1994).
[12] R. Auhl, R. Everaers, G. S. Grest, K. Kremer, and S. J. Plimpton, J. Chem. Phys. **119**, 12718 (2003).
[13] J. Gao, J. Chem. Phys. **102**, 1074 (1995).
[14] M. Perez, O. Lame, F. Leonforte, and J.-L. Barrat, J. Chem. Phys. **128**, 234904 (2008).
[15] N. C. Karayiannis, V. G. Mavrantzas, and D. N. Theodorou, Phys. Rev. Lett. **88**, 105503 (2002).
[16] V. G. Mavrantzas, T. D. Boone, E. Zervopoulou, and D. N. Theodorou, Macromolecules **32**, 5072 (1999).
[17] P. K. Pant and D. N. Theodorou, Macromolecules **28**, 7224 (1995).
[18] N. C. Karayiannis, A. E. Giannousaki, V. G. Mavrantzas, and D. N. Theodorou, J. Chem. Phys. **117**, 5465 (2002).
[19] A. Uhlherr, M. Doxastakis, V. G. Mavrantzas, D. N. Theodorou, S. J. Leak, N. E. Adam, and P. E. Nyberg, Europhys. Lett. **57**, 506 (2002).
[20] N. C. Karayiannis, A. E. Giannousaki, and V. G. Mavrantzas, J. Chem. Phys. **118**, 2451 (2003).
[21] L. D. Peristeras, I. G. Economou, and D. N. Theodorou, Macromolecules **38**, 386 (2005).
[22] J. Ramos, L. D. Peristeras, and D. N. Theodorou, Macromolecules **40**, 9640 (2007).
[23] K. C. Daoulas, A. F. Terzis, and V. G. Mavrantzas, J. Chem. Phys. **116**, 11028 (2002).
[24] K. C. Daoulas, A. F. Terzis, and V. G. Mavrantzas, Macromolecules **36**, 6674 (2003).
[25] G. Subramanian, J. Chem. Phys. **133**, 164902 (2010).
[26] G. Subramanian, Macromol. Theory Simul. **20**, 46 (2011).
[27] G. Zhang, L. A. Moreira, T. Stuehn, K. C. Daoulas, and K. Kremer, ACS Macro. Lett. **3**, 198 (2014).
[28] L. A. Moreira, G. Zhang, F. Müller, T. Stuehn, and K. Kremer, Macromol. Theory Simul. **24**, 419 (2015).
[29] D. N. Theodorou and U. W. Suter, Macromolecules **18**, 1467 (1985).
[30] D. N. Theodorou and U. W. Suter, Macromolecules **19**, 139 (1986).
[31] P. Carbone, H. A. Karimi-Varzaneh, and F. Müller-Plathe, Faraday Discuss. **144**, 25 (2010).
[32] M. Kotelyanskii, N. Wagner, and M. E. Paulaitis, Macromolecules **29**, 8497 (1996).
[33] Y. R. Sliozberg, M. Kröger, and T. L. Chantawansri, J. Chem. Phys. **144**, 154901 (2016).
[34] G. S. Grest and K. Kremer, Phys. Rev. A **33**, 3628 (1986).
[35] C. Svaneborg, H. A. Karimi-Varzaneh, N. Hojdis, F. Fleck, and R. Everaers, arXiv:1606.05008.
[36] A. Rosa and R. Everaers, Phys. Rev. Lett. **112**, 118302 (2014).
[37] P. J. Hoogerbrugge and J. M. V. A. Koelman, Europhys. Lett. **19**, 155 (1992).
[38] P. Espanol and P. Warren, Europhys. Lett. **30**, 191 (1995).
[39] P. J. Flory, J. Chem. Phys. **17**, 303 (1949).
[40] P. J. Flory, *Statistical Mechanics of Chain Molecules* (Wiley, New York, 1969).
[41] S. F. Edwards, Proc. Phys. Soc. **92**, 9 (1967).
[42] P. E. Rouse, J. Chem. Phys. **21**, 1272 (1953).

[43] R. Everaers, Phys. Rev. E. **86**, 022801 (2012).
[44] K. Kremer and G. S. Grest, J. Chem. Phys. **92**, 5057 (1990).
[45] R. Faller, A. Kolb, and F. Müller-Plathe, Phys. Chem. Chem. Phys. **1**, 2071 (1999).
[46] R. Faller, F. Müller-Plathe, and A. Heuer, Macromolecules **33**, 6602 (2000).
[47] R. Faller and F. Müller-Plathe, ChemPhysChem **2**, 180 (2001).
[48] N. Grønbech-Jensen and O. Farago, Mol. Phys. **111**, 983 (2013).
[49] N. Grønbech-Jensen, N. R. Hayre, and O. Farago, Comput. Phys. Commun. **185**, 524 (2014).
[50] S. Plimpton, J. Comput. Phys. **117**, 1 (1995).
[51] S. K. Sukumaran, G. S. Grest, K. Kremer, and R. Everaers, J. Polym. Sci., Part B: Polym. Phys. **43**, 917 (2005).
[52] L. J. Fetters, D. J. Lohse, and R. H. Colby, in *Physical Properties of Polymers Handbook*, edited by J. Mark (Springer, New York, 2007), p. 447.
[53] Q. Wang, Soft Matter **5**, 4564 (2009).
[54] E. Helfand and Y. Tagami, J. Polym. Sci. B **9**, 741 (1971).
[55] E. Helfand and Y. Tagami, J. Chem. Phys. **56**, 3592 (1972).
[56] N. Madras and A. D. Sokal, J. Stat. Phys. **50**, 109 (1988).
[57] Software available upon request from C. Svaneborg.
[58] J. P. Wittmer, P. Beckrich, A. Johner, A. N. Semenov, S. P. Obukhov, H. Meyer, and J. Baschnagel, Europhys. Lett. **77**, 56003 (2007).
[59] J. P. Wittmer, P. Beckrich, H. Meyer, A. Cavallo, A. Johner, and J. Baschnagel, Phys. Rev. E **76**, 011803 (2007).
[60] P. Beckrich, A. Johner, A. N. Semenov, S. P. Obukhov, H. Benoit, and J. P. Wittmer, Macromolecules **40**, 3805 (2007).
[61] H. Meyer, J. P. Wittmer, T. Kreer, P. Beckrich, A. Johner, J. Farago, and J. Baschnagel, Eur. Phys. J. E **26**, 25 (2008).
[62] A. N. Semenov, Macromolecules **43**, 9139 (2010).
[63] S. W. Sides, G. S. Grest, M. J. Stevens, and S. J. Plimpton, J. Polym. Sci., Part B: Polym. Phys. **42**, 199 (2004).
[64] R. S. Hoy, K. Foteinopoulou, and M. Kröger, Phys. Rev. E **80**, 031803 (2009).
[65] N. Uchida, G. S. Grest, and R. Everaers, J. Chem. Phys. **128**, 044902 (2008).
[66] G. Zhang, T. Stuehn, K. C. Daoulas, and K. Kremer, J. Chem. Phys. **142**, 221102 (2015).
[67] R. S. Hoy and M. O. Robbins, Phys. Rev. E **72**, 061802 (2005).
[68] Hardware setup of the Abacus 2.0 cluster at the University of Southern Denmark, https://deic.sdu.dk/setup/hardware, 2016.
[69] C. Svaneborg and J. S. Pedersen, J. Chem. Phys. **136**, 104105 (2012).
[70] C. Svaneborg and J. S. Pedersen, J. Chem. Phys. **136**, 154907 (2012).
[71] P. Debye, J. Phys. Colloid Chem. **51**, 18 (1947).
[72] B. Hammouda, J. Polym. Sci., Part B: Polym. Phys. **30**, 1387 (1992).